Effects of urban eutrophication on pelagic habitat capacity in the Southern California Bight

Christina A. Frieder[1,*], Fayçal Kessouri[1], Minna Ho[1,2], Martha Sutula[1], Daniele Bianchi[2], James C. McWilliams[2], Curtis Deutsch[3], and Evan Howard[3]

[1]Southern California Coastal Water Research Project, Costa Mesa, 92626, USA
[2]University of California Los Angeles, Los Angeles, 90095, USA
[3]Princeton University, Princeton, 08544, USA
[*]christinaf@sccwrp.org

ABSTRACT

Land-based nutrient inputs to the ocean have been linked to increased coastal productivity, subsurface acidification and O_2 loss, even in upwelling systems like the Southern California Bight. However, whether eutrophication alters the capacity to support key taxa has yet to be evaluated for this region. Here, we assess the impact of land-based nutrient inputs on the availability of aerobic and calcifying habitat for key pelagic taxa using ocean model simulations. We find that acute, lethal conditions are not commonly induced in epipelagic surface waters, but that sublethal, ecologically relevant changes are pervasive. Land-based nutrient inputs reduce the potential aerobic and calcifier habitat during late summer, when viable habitat is at its seasonal minimum. A region of annually recurring habitat compression is found 30 – 90 km from the mainland, southeast of Santa Catalina Island. Here, both aerobic and calcifier habitat is vertically compressed by, on average, 25%, but can be as much as 60%. This effect can be traced to enhanced remineralization of organic matter that originates from the coast. These findings suggest that effects of land-based nutrients are not restricted to chemistry but extend to habitat capacity for multiple taxa of ecological and economic importance. Considerable uncertainty exists, however, in how this habitat compression translates to population-level effects.

Introduction

Global change is fundamentally restructuring marine ecosystems, shifting distributions, phenologies, and interactions among species. Temperature (T), oxygen (O_2), and carbonate chemistry (e.g., pH, Ω_{Ar}) naturally constrain available habitat for marine calcifiers and aerobic animals, but as ocean waters warm, become less oxygenated, and more acidified, these changes are driving habitats beyond the envelope of natural variability, resulting in major changes to species distribution and abundance, and raising the potential for major ecosystem disruptions[1,2]. While shifts in species abundance or geographic range can be detected in historical data, local human impacts from nitrogen pollution and coastal eutrophication confound the attribution of biological changes to long-term climate trends. Effective coastal ecosystem management in the face of global change requires the means to both: (1) quantify these fundamental changes to species habitats and (2) disentangle the relative roles of climate change, natural and climatic variability, and local anthropogenic pressures in shaping those habitats. Ocean numerical models are routinely used to project the effects of climate change on shifting habitats and species distributions[3], but few coastal numerical modeling studies have investigated the potential for local coastal eutrophication to constraint marine calcifier and aerobic habitat[4]. As 50% of the global wastewater receives no treatment before discharging to coastal waters, such studies can help to understand whether local management of coastal eutrophication could meaningfully increase resilience of ecosystems to climate change.

Effects of eutrophication on increased primary productivity, enhanced remineralization rates, subsurface O_2 depletion, and acidification are commonly observed within the 100-m isobath, in semi-enclosed seas, and estuaries[5,6]. However, recent work has revealed that such changes can be meaningful even in upwelling-dominated coastal environments, countering the tenet that low O_2 and Ω_{Ar} that occur along eastern boundary upwelling systems is naturally induced, without direct anthropogenic influence[7]. In the Southern California Bight (SCB), coastal nitrogen export from a human population of 22 million rival natural upwelling in magnitude, roughly doubling available nitrogen[8]. These inputs, which include point and nonpoint source discharges to the ocean from 19 ocean outfalls and 75 rivers, which release, on average, 8 million m^3 d^{-1} of nutrient-enriched water to the ocean[9], are increasing primary production and subsurface respiration rates along the coast, with corresponding subsurface reductions in O_2 and aragonite saturate state (Ω_{Ar}) that rival or exceed that of global open-ocean O_2 loss and acidification since the pre-industrial period[10].

While Kessouri et al.[10] quantified the change in seawater chemistry from anthropogenic nutrient inputs in the Bight, it did not document the potential for biological effects, a fundamental science gap that motivates coastal water quality managers. In the SCB, these changes in seawater chemistry can extend more than 100 km from the coast ($\sim$30% of the Bight)[11]. The region of maximum change occurs in the epipelagic zone, localized between 50 and 200 m water depth. When these declines are superimposed on areas already naturally low in O_2 and Ω_{Ar}, even small changes could be of biogeochemical and ecological significance[12,13]. The question is whether these subsurface O_2 and acidification changes are occuring at ecologically relevant conditions, resulting in vertical compression of habitat. There are field-based demonstrated consequences of coastal acidification for shell-building zooplankton, in particular pteropods[14]. Similarly, O_2 depletion in the ocean can reduce metabolic performance of aerobic taxa[15–17]. Most of the literature on hypoxia focuses on acute lethal levels, but sublethal effects, even subtle ones that pose constraints on feeding times, can combine to limit growth or reproduction[2,18]. Studies in other ecosystems have documented how short-term, low-O_2 events can give rise to immediate habitat compression of sensitive species, increasing susceptibility to overfishing (e.g. of brown shrimp and demersal fishes in the Gulf of Mexico[19] and of artisanal fisheries species in the Sea of Oman[20]). Even the behavior of smaller vertical-migrating taxa, like copepods, is shaped by seasonal O_2 and temperature[21]. On the longer-term, interactions between temperature and O_2 availability on aerobic metabolism have strong correspondence with faunal diversity, species distributions, predator-prey interactions, and changing biogeographic patterns[22–24], and may even result in range shifts[1,2] and extinction[3].

In this study, we assess the degree to which modeled O_2 losses and acidification due to land-based nutrient inputs translates to changes in habitat capacity. To accomplish this, we rely on two metrics that define the habitat available for aerobic metabolism and for calcification. Aerobic habitat is determined using the Metabolic Index (Φ), whose trait-based threshold varies across species. Aerobic habitat for northern anchovy, *Engrualis mordax*, is detailed but we also consider how aerobic habitat is modified across the full range of metabolic traits. Calcifying habitat is based on the saturation state of aragonite (Ω_{Ar}), whose thresholds also vary among species. We evaluate calcifier habitat capacity as the thickness of the water column where $\Omega_{\mathrm{Ar}} \geq 1.4$, but we also consider the sensitivity of our results to other values of Ω_{Ar}. Our study objectives are threefold. First, we evaluate temporal and spatial patterns in aerobic and calcifier habitat capacity metrics in the SCB with output from a 20-year numerical ocean model hindcast. Second, we test how anthropogenic nutrient inputs from land-based sources alter the vertical thickness of the habitat capacity metrics. We rely on two model scenarios, the first includes natural oceanic cycles of nutrients, O_2 and carbon, to which rising global CO_2 emissions have been imposed (referred to hereafter as 'CTRL'), and the second includes both natural oceanic cycles of nutrients with inputs from terrestrial sources, 98%

of which are anthropogenic and 95% of which are point source in origin (referred to hereafter as 'ANTH')[9]. Third, we confirm the mechanisms by which anthropogenic nutrients contribute to the observed changes in vertical habitat capacity by analyzing changes in the biogeochemical rate processes that contribute to the O_2 and carbon cycle.

Results

For both habitat capacity metrics, there are consistent Bight-wide spatial and temporal patterns (Fig.1), with calcifier habitat thickness greater than anchovy aerobic habitat thickness. Calcifier habitat thickness ranges from, on average, 80 to 130 m. Anchovy aerobic habitat thickness ranges, on average, from 50 to 100 m. Both habitat thickness metrics are most restricted within the Santa Barbara Channel and around San Nicolas Island. Increases generally occur along north-to-south and onshore-to-offshore gradients.

The dominant temporal scales of calcifier and anchovy aerobic habitat capacity are inter-annual and seasonal (Fig.1). The temporal mean of total calcifier and anchovy aerobic habitat volumes are 8.2 and 5.4 x 10^3 km^3, respectively, summed across the model domain. Among years, total volume for each metric can vary approximately 2-fold. In 2011, calcifier and anchovy aerobic habitat volumes were most restricted at 4.2 and 3.6 x 10^3 km^3; in 1998, habitat volumes were most expansive at 10.2 and 6.2 x 10^3 km^3, respectively. Seasonal variability also drives approximately 2-fold changes in habitat volumes. An evaluation of the annually detrended time series for both metrics shows that total habitat volumes are greatest during winter months and contract during summer, with the least amount of total habitat available during July and August (Fig.1D-E). Since anchovy aerobic habitat is constrained by both temperature and O_2, attribution analysis reveals that O_2 is the primary contributor to seasonal trends in total habitat volume, and that seasonal changes in temperature counteract that of O_2 (Fig. S1).

There is not a consistent tendency for land-based nutrient inputs to result in consistent or persistent Bight-wide calcifier and aerobic habitat capacity gains or losses (Fig. S2). The relative, Bight-wide differences in total habitat volume vary by $\pm$ 5% for most of the period simulated. However, at any grid cell location, the difference in calcifier habitat thickness between ANTH and CTRL can range from -34 to $+45$%, and that for anchovy aerobic habitat ranges from -43 to $+80$% (1^{st} and 99^{th} percentiles, respectively).

A spatial perspective of the change in calcifier and anchovy aerobic habitat thickness reveals a region of habitat loss that is expressed southeast of Santa Catalina Island (Fig. S2). This region of habitat loss is a seasonal phenomenon. In seven of the nine years simulated, there is a compression event lasting approximately 2.5 months that occurs in the late summer to early fall (Fig. 2c-d), a time period when calcifier and anchovy aerobic habitat thickness are already seasonally compressed (Fig. 1d-e). Averaging across these seven compression events, the total spatial area experiencing recurrent calcifier habitat change is 2,364 km^2 (assessed as the total spatial area where the change in calcifier habitat thickness ≤ -20%; Fig. 2a) The equivalent total spatial area experiencing recurrent anchovy aerobic habitat change is 1,909 km^2 (Fig. 2b). Despite the temporal overlap in natural seasonal and eutrophication-driven compression, there is spatial mismatch between the regions undergoing maximum habitat compression due to eutrophication with those that are naturally most restricted from broad-scale oceanographic patterns (e.g., Santa Barbara Channel; Fig. 1a-b).

Anchovy represent one ecophysiotype in a range of metabolic trait possibilities. Quantifying aerobic habitat change across the full range of Metabolic Index trait combinations (E_o and A_o/Φ_{CRIT}) demonstrates that not all ecophysiotypes are subject to aerobic habitat loss (Fig. 3A). Ecophysiotypes with higher

hypoxia tolerance (A_o/Φ_{CRIT}) gain aerobic habitat volume; while those with lower hypoxia tolerance, including anchovy, lose aerobic habitat volume. Taking a species-weighted distribution of metabolic trait possibilities, approximately two-thirds of species are losing aerobic habitat volume, and the modeled losses can be up to three times greater than the gains (Fig. 3b). Of those subjected to aerobic habitat loss, 70% of species are subject to more habitat loss than northern anchovy (Table S1). These species that are gaining aerobic habitat volume have higher hypoxia tolerance at any given temperature sensitivity (E_o; Fig. 3a), with the biggest gain in aerobic habitat volume available for Humboldt squid, *Dosidicus gigas* (Table S1).

The spatial and vertical distribution of greatest O_2 change is occurring between approximately 40 and 100 km from the coast and between 50 and 150 meters or more below the surface (Fig. 4b). The same pattern is observed for acidification, assessed as the difference in Ω_{Ar} between the two scenarios (Fig. 4b). The lower limit of anchovy aerobic habitat coincides in space with the region of maximum O_2 loss. In the CTRL scenario, the anchovy aerobic habitat limit is at 80 m in the offshore region of maximum O_2 loss (60 km from the coast), and shoals to 60 m in the ANTH scenario. In contrast, the lower limit for calcifier habitat thickness is deeper than the vertical region undergoing maximum acidification. Still, calcifier habitat thickness shoals from approximately 115 m in the CTRL scenario to 87 m in the ANTH scenario. Because both subsurface acidification and O_2 loss occur across a broad depth range, our results are largely insensitive to which value of Ω_{Ar} is used to define optimal calcifier habitat (Fig. S3). Similarly, loss of O_2 is occurring across a broad depth range (Fig. S4). Notably, these changes to habitat capacity in the epipelagic are largely limited to sublethal effects as conditions that trigger acute lethal effects occur deeper in the water column. Conditions where Ω_{Ar} are less than 1 occur, on average, deeper than 200 m water depth (Fig. S3). Similarly, acute lethal O_2 conditions ($\Phi = 1$) for northern anchovy occurs, on average, much deeper than 300 m water depth, well below the typically observed vertical distributions of anchovy and other pelagic fishes.

Of the biogeochemical rate processes contributing to habitat change within the region of 20% habitat compression, remineralization rates are exhibiting the greatest absolute change due to land-based nutrient inputs (Fig. 5). For the carbon cycle, remineralization rates increase from 4.26 ± 0.12 to 4.50 ± 0.12 mmol DIC m^{-3} d^{-1} from the CTRL to the ANTH scenario (mean $\pm$ 1 SE; N = 104 months). The increase in DIC from land-based nutrient inputs at the core of habitat compression drives the modeled decrease in Ω_{Ar}. Small changes in alkalinity (< 5 mmol m^{-3}) counteract the effects due to DIC (Fig. S5). For the O_2 cycle, remineralization rates are also exhibiting the greatest change due to land-based nutrient inputs, changing from -5.44 ± 0.15 to -5.75 ± 0.15 mmol O_2 m^{-3} d^{-1} from CTRL to ANTH (mean $\pm$ 1 SE; N = 104 months).

Discussion

Here, we demonstrate that eutrophication effects of land-based nutrient export to the Southern California Bight are not restricted to changes in seawater acidification and O_2 loss[11], but also extend to the potential for widespread effects on calcifier and aerobic habitat capacity. The seawater chemistry changes that occur in the epipelagic are not at conditions that elicit acute, lethal effects. However, the habitat capacity metrics used here are sensitive to eutrophication, changes recurring annually despite large, natural seasonal and interannual cycles (Fig. 1). During the late summer, subsurface acidification and O_2 loss routinely compress aerobic and calcifier habitat capacity (Fig. 2), at a time period when habitat capacity is already seasonally compressed (Fig. 1). Modeled habitat compression is most pronounced where excess nutrients and organic matter, which originate at the coast, are received and entrained within offshore eddies[11]. Since

seawater chemistry changes due to enhanced remineralization are occurring across a large depth range, patterns in habitat compression are largely insensitive to the value of Ω_{Ar} used to define the calcifier habitat capacity metric (Fig. S3). Similarly, while we evaluate aerobic habitat capacity for northern anchovy, we confirm that this pattern is consistent among two thirds of ecophysiotypes (although at differing magnitudes of loss), and that those species gaining aerobic habitat volume have higher active tolerances to low O_2 (Fig. 3).

There is field-based evidence that the vertical structure of both Ω_{Ar} and O_2 have implications for a variety of pelagic taxa. For example, across frontal gradients in the California Current System where Ω_{Ar} between 1.0 and 1.4 can shoal by 100+ m on the scale of tens of kms, there are concurrent reductions in pteropod abundance accompanied by elevated shell dissolution[25]. From onshore-to-offshore gradients, more severe pteropod shell dissolution and thinner shells occur close to the coast, particularly where upwelling is more intense[26,27]. The predicted habitat compression described here coincides with the natural seasonal cycle of limited habitat availability. Multiple species of pteropods, including *Limacina helicina*, are present year-round in the SCB (K. McLaughlin, pers. comm.). While limited baseline information on pteropod life history characteristics exist for the Southern California Bight[28], studies suggested that spring (April-May) and fall (September- October) are periods when early life stage cohorts are most vulnerable to changing ocean conditions[29–31].

Ocean O_2 depletion adversely impacts marine species, assemblages, and even fisheries[32]. Long-term deoxygenation trends play a role in, for example, declines in abundance of mesopelagic fishes[33] and shifts in zooplankton and small nekton diel migration depth[34]. Interactive effects of sub-optimal O_2 and temperature are becoming increasingly considered[13]. Sub-optimal O_2 stress depends on the O_2 supply relative to metabolic demand, and water temperature controls both chemical (O_2 solubility, diffusivity) and physiological processes (metabolic demand, ventilations rates) affecting this balance for marine ectotherms. We use the mechanistic framework of the Metabolic Index[22] to incorporate these dependencies into the index of aerobic habitat capacity. Specific to our focal taxa, northern anchovy have seasonal to interdecadal redistributions that correlate with aerobic habitat capacity. For example, anchovy migrate offshore during peak upwelling seasons[35,36], when nearshore aerobic habitat availability is lowest, even though their food supply is generally higher closer to the coast[1]. Further, the southern biogeographic limit of this species is coincident with the aerobic habitat capacity threshold implied by their oscillations in time within the SCB, and vice versa[1]. While reductions in this index are associated with species-specific consequences of deoxygenation at the regional scale, it remains unclear how the spatial and seasonal extent of the O_2 reduction identified here might translate to disruptions across species of varying phenologies, mobility, and ecological niches. The same can be said for the population-level consequences of subsurface acidification.

We evaluate O_2 loss and acidification effects on habitat capacity separately, as the combined effects of these stressors on biological responses are insufficiently understood[4]. However, studies suggest that exposure to suboptimal ranges of acidification, O_2, and temperature can make marine organisms more sensitive to O_2 loss[37] or less resilient to acidification[38]. In this model domain, there is strong covariance between calcifier and aerobic habitat thickness (Pearson correlation coefficient = 0.79), linked to eutrophication effects on water-column remineralization, such that aerobic and calcifier habitat compress at the same time. Thus, predicted effects on habitat capacity for marine species may be underestimated[4]. The Metabolic Index framework does incorporate the combined effects of temperature and O_2. Biological sensitivities to all three variables – temperature, O_2, and carbonate system state – could potentially be merged through a fundamental physiological trait such as aerobic scope (i.e., a proxy for the surplus energy available for

growth, reproduction, predator avoidance, etc.).

While we emphasize subsurface losses in habitat capacity, anthropogenic nutrient loads can also enhance productivity and food supply in coastal ecosystems, thereby potentially reducing the negative consequences of suboptimal O_2 and acidification[39,40]. As an example, total fisheries landings can remain high even if demersal species in O_2-depleted areas decline, because nutrients can stimulate prey production in other well-mixed parts of a system[39,41]. Abundant prey can improve stress tolerance of organisms[42]. However, system-wide compensation through enhanced productivity will have limits as the volume of O_2-depleted waters expand[43]. The catch per unit effort for selected demersal fish species along the U.S. West Coast is positively related to near-bottom O_2 concentrations, with the catch per unit effort decreasing more significantly as O_2 concentrations decrease[44]. In the Humboldt Current, it is suggested that low O_2 near the coast results in a highly efficient trophic transfer and a dense anchovy population[45], which is beneficial for fishing activities. During these conditions, species that are less tolerant to low O_2, like sardine and jack mackerel, are restricted to offshore, well-oxygenated waters[46,47].

Global climate change will further exacerbate habitat loss resulting from land-based nutrient inputs[10]. Strengthened stratification, from increased surface water temperatures as the global climate warms, is sufficient to worsen subsurface O_2 and acidification where it currently exists and may instigate habitat loss elsewhere[48]. Warming and O_2 loss by 2100 are projected to result in complete loss of aerobic habitat for northern anchovy – and thus likely extirpation – from the southern California Current System (CCS)[1]. Further, the interplay of anthropogenic nutrient export and stratification where they occur could accelerate the timeline of habitat compression and potential extirpation. In this study, O_2 loss in the core of habitat compression exceeds 30 μmol kg^{-1} (Fig. 4c). This is 1.5 times the scale of decadal O_2 loss in the southern CCS which may be occurring at around 20 μmol kg^{-1} $decade^{-1}$[49]. Acidification in the same eutrophication-induced core exceeds -0.3 units for Ω_{Ar}, and this is three times the decadal trend of approximately -0.1 $decade^{-1}$[50,51].

To conclude, we assess change in habitat capacity for pelagic calcifying and aerobic taxa due to eutrophication effects on subsurface acidification and O_2 loss from land-based nutrients. Our findings suggest that effects of land-based nutrients are not restricted to chemistry. Changes to habitat capacity defined by sublethal, ecologically relevant thresholds were pervasive during late summer, when habitat capacity is at its seasonal minimum. Despite the theoretical, experimental, and field evidence that identify the importance of the vertical structure of both carbonate chemistry and O_2 for marine pelagic communities, whether the modeled habitat compression shown here translate to population-level effects is uncertain. Actions to increase this certainty can include the expansion of a habitat capacity metric that includes the interactive effects of acidification and O_2 loss, consideration of how these outcomes interplay with food availability, and investigation into the scales at which spatial and temporal changes in habitat capacity translate to population-level effects. All of which can be bolstered by robust, region-wide modeling, experimental, and field programs.

Methods

To assess whether modeled effects of land-based nutrient inputs on Bight-wide subsurface O_2 loss and acidification are biologically relevant, we employed two metrics for habitat capacity, which we adapted for this purpose. One incorporates temperature-dependent environmental O_2 as a predictor of habitat capacity for aerobic metabolism and the other incorporates carbonate chemistry as a predictor of habitat capacity for aragonite production by calcifiers. The premise of our approach is that these metrics provide information on the capacity of a specified location to provide habitat conditions that are sufficient for key

processes for a species, or group of species, based on either empirical or mechanistic relationships of organismal performance with the environmental condition(s) of interest. The habitat capacity metrics are applied to model outputs from scenarios with and without land-based nutrient inputs in order to perform a difference assessment. Each metric is presented as the volume or vertical thickness of water-column as spatial gradients in both O_2 and carbonate chemistry are greatest in the vertical dimension.

Since modeled effects of subsurface O_2 loss and acidification due to anthropogenic nutrient inputs are shown to be localized between 50 and 200 m[11], we focus our analysis on pelagic taxa. Because literature is limited on the interactive effects of O_2 and carbonate chemistry in these environments, we adapt two separate metrics to evaluate the changes in O_2 versus the changes in carbonate chemistry with an emphasis on aerobic taxa and calcifiers, accordingly.

For the effects of subsurface acidification on calcifier habitat capacity, we calculate the vertical thickness of optimal aragonite saturation state (Ω_{Ar}) conditions. A value of Ω_{Ar} of 1.4 is used to define the condition below which sublethal organismal responses have been documented to commonly occur[14,52,53]. One of the primary lines of evidence for this choice is derived from a synthesis of documented effects on pteropods[14], in which Ω_{Ar} thresholds for a range of sublethal to lethal responses were identified and confidence in thresholds were judged with expert consensus. Pteropods are ubiquitous, holoplanktonic calcifiers that have a well-documented, specific sensitivity to ocean acidification. These calcifiers efficiently transfer energy from phytoplankton to higher trophic levels[54,55], and as such serve as an important prey group for ecologically and economically important fishes, bird, and whale diets[56–58]. Bednaršek et al.[14] identified that Ω_{Ar} from 1.5 – 0.9 provides a risk range from mild dissolution to lethal impacts. Our selected value of Ω_{Ar} of 1.4 represents a value within observational analytical precision ($\pm$ 0.2[59]) of thresholds where sublethal effects on calcification, growth, and severe dissolution are documented to occur, while a value of 1.0 roughly equates to lethal effects (0.9 to 0.95[14]). In the epipelagic (0-200 m), conditions below saturation have not been common in the modern ocean but are predicted to emerge as soon as the 2030's and 2040's[60]. Importantly, we perform an analysis of the sensitivity of our findings to the choice of Ω_{Ar} along this range of 1.0 to 1.4 and find the results to be largely sensitive within this range (see Analytical Approach for further details).

For the effects of subsurface O_2 loss on aerobic habitat capacity, we calculate the vertical thickness of the water column that has sufficient O_2 to provide ecological support for northern anchovy (*Engraulis mordax*). Northern anchovy is also holoplanktonic with greatest abundance observed in the upper 100 m[35]. Defining sufficient O_2 for ecological support relies on the mechanistic framework of the Metabolic Index (Φ[22,23]). Φ is defined as the ratio of O_2 supply to resting demand. We can calculate the habitat thickness for which $\Phi/\Phi_{CRIT} \geq 1$, a value below which demarcates environment in which anchovy can sustain resting but not active energetic demands, thus limiting population persistence. For northern anchovy, metabolic traits have been inferred from observational datasets associated with climatological O_2 and temperature conditions[1]. While we use metabolic traits for northern anchovy as our primary analysis, we consider how modeled O_2 loss interacts with the full range of metabolic trait combinations. Similarly, we evaluate a lethal threshold for northern anchovy, where $\Phi = 1$ and O_2 supply is insufficient to meet O_2 demand. This latter analysis converts the reported active hypoxia threshold (A_o/Φ_{CRIT}) to the value at rest (A_o) using $\Phi_{CRIT} = 3.5$, the mean value across marine organisms (Deutsch et al. 2020); some species have Φ_{CRIT} as low as 1.5, in which case the lethal thresholds could occur at proportionately higher values of O_2 and thus at shallower depths.

We utilize biogeochemical output from the Regional Ocean Modeling System, ROMS[61], coupled to the Biogeochemical Elemental Cycling model, BEC[62], which has been adapted for the CCS[63,64]. BEC is a

multi-element (C, N, P, O, Fe, and Si) and multi-plankton model that includes three explicit phytoplankton functional groups (picoplankton, silicifying diatoms, and N-fixing diazotrophs), one zooplankton group, and dissolved and sinking organic detritus. Remineralization of sinking organic material follows the multi-phase mineral ballast parameterization of Armstrong et al.[65], and sedimentary processes have also been expanded. Particulate organic matter reaching the sediment is accumulated and remineralized with a time scale of 330 days, to provide a buffer between particle deposition and nutrient release. The ecosystem is linked to a carbon system module that tracks dissolved inorganic carbon and alkalinity, and an air–sea gas exchange module based on the formulation of Wanninkhof[66].

The SCB model domain, which extends from Tijuana Mexico to Pismo Beach (U.S. Central California coast) and about 200-km offshore, is part of a nested configuration. Model nests scale from a 4-km horizontal resolution configuration spanning the entire CCS, to a 1-km resolution grid covering much of the California coast (latitude < 40.25°N), to a 0.3-km grid in the SCB, where our investigations of local anthropogenic inputs were focused[10,67]. This grid, shown in Fig. 1a, is composed of 1,400 × 600 grid points, with 60 σ-coordinate vertical levels using the stretching function described in Shchepetkin and McWilliams[61]. The model is run with a time step of 30 s, and outputs are saved as 1-day averages. More information on the model setup and forcing is provided in other works[63,64,67].

ROMS-BEC has been validated for atmospheric forcing, physics, and biogeochemistry including O_2, carbonate saturation state, primary productivity, and hydrographic parameters at a West Coast-wide scale[63] and, within the SCB, at scales at which anthropogenic nutrients inputs influence coastal eutrophication[67].

We rely on two model scenarios. The first includes only natural oceanic cycles of nutrients (CTRL) and thus represents only natural ocean cycles of nutrient, carbon, and O_2, with the effects of global CO_2 superimposed. The second represents these same CTRL base conditions, to which inputs from terrestrial sources are added, 98% of which are anthropogenic and 95% of which are point source in origin (ANTH)[9]. Model simulations that include terrestrial inputs were forced with a monthly time series of spatially explicit inputs, including freshwater flow, nitrogen, phosphorus, silica, iron, and organic carbon representing natural and anthropogenic sources[9]. These data include POTW ocean outfalls and riverine discharges (1997–2017) and spatially explicit modeled estimates of atmospheric deposition. POTW effluent data were compiled from permit monitoring databases and communication with sanitary agencies. Monthly time series of surface water runoff from 75 rivers are derived from model simulations and monitoring data[9]. The CTRL simulation covers the time periods of 02/1997 – 01/2001 and 08/2012 – 11/2017. The ANTH simulation covers the time period of 02/1997 – 11/2017.

Aragonite saturation state was computed with the CO2SYS algorithms[68,69] using daily averages of model output fields of dissolved inorganic carbon (DIC), total alkalinity (TA), temperature, salinity, and pressure. Calcifier habitat thickness was calculated as the thickness of the water column for each grid cell that was $\geq$ optimal Ω_{Ar} (1.4) for pteropods.

The ecological Metabolic Index (Φ/Φ_{CRIT}) was computed from daily averages of model output fields of O_2 and temperature.

$$\frac{\Phi}{\Phi_{CRIT}} = \frac{A_o}{\Phi_{CRIT}} \times \frac{pO_2}{exp(-E_o/k_B(1/T - 1/T_{ref}))} \tag{1}$$

The metabolic traits of northern anchovy are A_o/Φ_{CRIT} = 5.4 atm^{-1} (equivalent to an active hypoxia threshold of pO_2 = 0.185 atm at 15°C) and E_o = 0.4 eV (the net temperature sensitivity of O_2 supple

and demand)[1]. pO_2 is the environmental partial pressure of O_2 and T is temperature (in K). k_B is the Boltzmann constant and T_{ref} is the reference temperature (here, 288.15 K). Aerobic habitat thickness was calculated as the thickness of the water column where $\Phi/\Phi_{CRIT} \geq 1$.

Spatial and temporal patterns in calcifier and aerobic habitat thickness were evaluated with the ANTH simulation to identify the dominant spatial and temporal scales of variability in each. Total calcifier and aerobic habitat for the model domain was summed across all grid cells as the habitat thickness within a grid cell multiplied by the area of that grid cell.

To then evaluate how anthropogenic nutrient inputs alter calcifier and aerobic habitat thickness, we perform a difference assessment (ANTH-CTRL) where positive (negative) values represent an expansion (contraction) of habitat thickness attributable to anthropogenic nutrient inputs included in the ANTH scenario only. We focus further analyses in regions where differences in habitat thickness exceed $\pm$ 20%. To test the sensitivity of calcifier habitat capacity to the value of Ω_{Ar}, we evaluate habitat thickness for $\Omega_{Ar} \geq 1.0 - 2.5$. We also calculate the change in water-column thickness for a range of $[O_2]$ from 60 – 200+ mmol m^{-3}. Since northern anchovy, our species of focus for aerobic habitat, is just one ecophysiotype among a range of possibilities, we evaluate the change in aerobic habitat volume across the full combination of metabolic trait possibilities (A_o/Φ_{CRIT} and E_o) and estimate the fraction of species undergoing trait-weighted volume changes with a probability distribution of empirical traits (derived by Penn and Deutsch[3]).

For regions undergoing more than a $\pm$ 20% change in habitat thickness, we evaluate the difference in the biogeochemical rate processes from each scenario (detailed methods provided in Deutsch et al.[63] and Kessouri et al.[11]). Biogeochemical rate processes that influence the O_2 cycle include surface air-sea flux, photosynthesis, non-grazing mortality, grazing mortality, water-column remineralization, sediment-water flux, NH_4 oxidation, and nitrification (Eq. A9 in Deutsch et al.[63]). Biogeochemical rate processes that influence dissolved inorganic carbon include air-sea flux, photosynthesis, $CaCO_3$ production, non-grazing mortality, grazing mortality, and water-column and sediment remineralization (Eq. A11 in Deutsch et al.[63]). We perform a difference assessment from the monthly averages for the sum of the biogeochemical process terms. This analysis is focused between 70 and 140-m water depth to align with the depth range where habitat thickness is affected.

References

1. Howard, E. M. *et al.* Climate-driven aerobic habitat loss in the California Current System. *Sci. Adv.* **6**, eaay3188 (2020).

2. Pinsky, M. L., Selden, R. L. & Kitchel, Z. J. Climate-driven shifts in marine species ranges: Scaling from organisms to communities. *Annu. Rev. Mar. Sci.* **12**, 153–179 (2020).

3. Penn, J. L. & Deutsch, C. Avoiding ocean mass extinction from climate warming. *Science* **376**, 524–526 (2022).

4. Bednaršek, N., Pelletier, G., Ahmed, A. & Feely, R. A. Chemical exposure due to anthropogenic ocean acidification increases risks for estuarine calcifiers in the salish sea: Biogeochemical model scenarios. *Front. Mar. Sci.* **7**, 580 (2020).

5. Rabalais, N. Eutrophication. In Robinson, A. R. & Brink, K. H. (eds.) *The Global Coastal Ocean: Multiscale Interdisciplinary Processes*, vol. 13, chap. 21, 821–866 (Harvard University Press, Cambridge, Massachusetts and London, 2005).

6. Rabalais, N. N., Turner, R. E., Díaz, R. J. & Justić, D. Global change and eutrophication of coastal waters. *ICES J. Mar. Sci.* **66**, 1528–1537, DOI: 10.1093/icesjms/fsp047 (2009).

7. Fennel, K. & Testa, J. M. Biogeochemical controls on coastal hypoxia. *Annu. Rev. Mar. Sci.* **11**, 105–130 (2019).

8. Howard, M. D. *et al.* Anthropogenic nutrient sources rival natural sources on small scales in the coastal waters of the Southern California Bight. *Limnol. Oceanogr.* **59**, 285–297 (2014).

9. Sutula, M. *et al.* A baseline of terrestrial freshwater and nitrogen fluxes to the Southern California Bight, USA. *Mar. Pollut. Bull.* **170**, 112669, DOI: https://doi.org/10.1016/j.marpolbul.2021.112669 (2021).

10. Kessouri, F. *et al.* Coastal eutrophication drives acidification, oxygen loss, and ecosystem change in a major oceanic upwelling system. *Proc. Natl. Acad. Sci.* **118**, e2018856118 (2021).

11. Kessouri, F. Large-scale response to urban eutrophication in the southern California Current System. (Submitted).

12. Levin, L. A. Manifestation, drivers, and emergence of open ocean deoxygenation. *Annu. Rev. Mar. Sci.* **10**, 229–260, DOI: 10.1146/annurev-marine-121916-063359 (2018).

13. Roman, M. R., Brandt, S. B., Houde, E. D. & Pierson, J. J. Interactive effects of hypoxia and temperature on coastal pelagic zooplankton and fish. *Front. Mar. Sci.* **6**, 139 (2019).

14. Bednaršek, N. *et al.* Systematic review and meta-analysis toward synthesis of thresholds of ocean acidification impacts on calcifying pteropods and interactions with warming. *Front. Mar. Sci.* **6**, 227 (2019).

15. Fry, F. The effect of environmental factors on the physiology of fish. In Hoar, W. & Randall, D. (eds.) *Environmental Relations and Behavior*, vol. 6 of *Fish Physiology*, 1–98, DOI: https://doi.org/10.1016/S1546-5098(08)60146-6 (Academic Press, 1971).

16. Pörtner, H. O. & Knust, R. Climate change affects marine fishes through the oxygen limitation of thermal tolerance. *Science* **315**, 95–97 (2007).

17. Seibel, B. A. Critical oxygen levels and metabolic suppression in oceanic oxygen minimum zones. *J. Exp. Biol.* **214**, 326–336, DOI: 10.1242/jeb.049171 (2011).

18. Gunderson, A. R. & Leal, M. A conceptual framework for understanding thermal constraints on ectotherm activity with implications for predicting responses to global change. *Ecol. Lett.* **19**, 111–120 (2016).

19. Craig, J. K. Aggregation on the edge: effects of hypoxia avoidance on the spatial distribution of brown shrimp and demersal fishes in the northern Gulf of Mexico. *Mar. Ecol. Prog. Ser.* **445**, 75–95 (2012).

20. Piontkovski, S. A. & Al-Oufi, H. S. Oxygen minimum zone and fish landings along the Omani shelf. *J. Fish. Aquatic Sci.* **9**, 294 (2014).

21. Pierson, J. J., Slater, W.-C. L., Elliott, D. & Roman, M. R. Synergistic effects of seasonal deoxygenation and temperature truncate copepod vertical migration and distribution. *Mar. Ecol. Prog. Ser.* **575**, 57–68 (2017).

22. Deutsch, C., Ferrel, A., Seibel, B., Pörtner, H.-O. & Huey, R. B. Climate change tightens a metabolic constraint on marine habitats. *Science* **348**, 1132–1135 (2015).

23. Deutsch, C., Penn, J. L. & Seibel, B. Metabolic trait diversity shapes marine biogeography. *Nature* **585**, 557–562 (2020).

24. Seibel, B. A. Cephalopod susceptibility to asphyxiation via ocean incalescence, deoxygenation, and acidification. *Physiology* **31**, 418–429 (2016).

25. Bednaršek, N. & Ohman, M. Changes in pteropod distributions and shell dissolution across a frontal system in the California Current System. *Mar. Ecol. Prog. Ser.* **523**, 93–103 (2015).

26. Feely, R. A. *et al.* Chemical and biological impacts of ocean acidification along the west coast of North America. *Estuarine, Coast. Shelf Sci.* **183**, 260–270 (2016).

27. Mekkes, L. *et al.* Pteropods make thinner shells in the upwelling region of the California Current Ecosystem. *Sci. Reports* **11**, 1731 (2021).

28. Manno, C. *et al.* Shelled pteropods in peril: assessing vulnerability in a high CO_2 ocean. *Earth-Science Rev.* **169**, 132–145 (2017).

29. Gannefors, C. *et al.* The arctic sea butterfly *Limacina helicina*: lipids and life strategy. *Mar. Biol.* **147**, 169–177 (2005).

30. Wang, K. *The life cycle of the pteropod Limacina helicina in Rivers Inlet (British Columbia, Canada)*. Ph.D. thesis, University of British Columbia (2014).

31. Wang, K., Hunt, B. P., Liang, C., Pauly, D. & Pakhomov, E. A. Reassessment of the life cycle of the pteropod *Limacina helicina* from a high resolution interannual time series in the temperate North Pacific. *ICES J. Mar. Sci.* **74**, 1906–1920 (2017).

32. Laffoley, D. & Baxter, J. M. *Ocean deoxygenation: Everyone's problem-Causes, impacts, consequences and solutions* (IUCN Gland, Switzerland, 2019).

33. Koslow, J. A., Goericke, R., Lara-Lopez, A. & Watson, W. Impact of declining intermediate-water oxygen on deepwater fishes in the California Current. *Mar. Ecol. Prog. Ser.* **436**, 207–218 (2011).

34. Bianchi, D., Galbraith, E. D., Carozza, D. A., Mislan, K. & Stock, C. A. Intensification of open-ocean oxygen depletion by vertically migrating animals. *Nat. Geosci.* **6**, 545–548 (2013).

35. Mais, K. F. Pelagic fish surveys in the California Current. *California Dep. Fish Game's Fish Bull.* (1974).

36. Laroche, J. L. & Richardson, S. Reproduction of northern anchovy, *Engraulis mordax*, off Oregon and Washington. *Fish. Bull* **78**, 603–618 (1980).

37. Breitburg, D. L., Baumann, H., Sokolova, I. M. & Frieder, C. A. Multiple stressors–forces that combine to worsen deoxygenation and its effects. In Laffoley, D. & Baxter, J. M. (eds.) *Ocean deoxygenation: everyone's problem. Causes, impacts, consequences and solutions* (International Union for Conservation of Nature and Natural Resources, 2019).

38. Stevens, A. M. & Gobler, C. J. Interactive effects of acidification, hypoxia, and thermal stress on growth, respiration, and survival of four North Atlantic bivalves. *Mar. Ecol. Prog. Ser.* **604**, 143–161 (2018).

39. Breitburg, D. L., Hondorp, D. W., Davias, L. A. & Diaz, R. J. Hypoxia, nitrogen, and fisheries: integrating effects across local and global landscapes. *Annu. Rev. Mar. Sci.* **1**, 329–349 (2009).

40. de Mutsert, K. *et al.* Exploring effects of hypoxia on fish and fisheries in the northern Gulf of Mexico using a dynamic spatially explicit ecosystem model. *Ecol. Model.* **331**, 142–150 (2016).

41. Nixon, S. W. & Buckley, B. A. "A strikingly rich zone"—nutrient enrichment and secondary production in coastal marine ecosystems. *Estuaries* **25**, 782–796 (2002).

42. Marigomez, I., Múgica, M., Izagirre, U. & Sokolova, I. M. Chronic environmental stress enhances tolerance to seasonal gradual warming in marine mussels. *PLoS One* **12**, e0174359 (2017).

43. Breitburg, D. Effects of hypoxia, and the balance between hypoxia and enrichment, on coastal fishes and fisheries. *Estuaries* **25**, 767–781 (2002).

44. Keller, A. A. *et al.* Occurrence of demersal fishes in relation to near-bottom oxygen levels within the California Current Large Marine Ecosystem. *Fish. Oceanogr.* **24**, 162–176 (2015).

45. Bertrand, A. *et al.* Oxygen: a fundamental property regulating pelagic ecosystem structure in the coastal southeastern tropical Pacific. *PloS one* **6**, e29558 (2011).

46. Alegre, A. *et al.* Diet diversity of jack and chub mackerels and ecosystem changes in the northern Humboldt Current system: A long-term study. *Prog. Oceanogr.* **137**, 299–313 (2015).

47. Bertrand, A. *et al.* 3-d habitat suitability of jack mackerel *Trachurus murphyi* in the Southeastern Pacific, a comprehensive study. *Prog. Oceanogr.* **146**, 199–211 (2016).

48. Long, M., Ito, T. & Deutsch, C. Oxygen projections for the future. In Laffoley, D. & Baxter, J. M. (eds.) *Ocean deoxygenation: everyone's problem. Causes, impacts, consequences and solutions* (International Union for Conservation of Nature and Natural Resources, 2019).

49. Bograd, S. J. *et al.* Oxygen declines and the shoaling of the hypoxic boundary in the California Current. *Geophys. Res. Lett.* **35** (2008).

50. Leinweber, A. & Gruber, N. Variability and trends of ocean acidification in the southern California Current System: A time series from Santa Monica Bay. *J. Geophys. Res. Ocean.* **118**, 3622–3633 (2013).

51. Turi, G., Lachkar, Z., Gruber, N. & Münnich, M. Climatic modulation of recent trends in ocean acidification in the California Current System. *Environ. Res. Lett.* **11**, 014007 (2016).

52. Bednaršek, N. *et al.* Synthesis of thresholds of ocean acidification impacts on decapods. *Front. Mar. Sci.* **8**, 651102 (2021).

53. Bednaršek, N. *et al.* Synthesis of thresholds of ocean acidification impacts on echinoderms. *Front. Mar. Sci.* **8**, 602601 (2021).

54. Lalli, C. M. & Gilmer, R. W. *Pelagic snails: The biology of holoplanktonic gastropod mollusks* (Stanford University Press, 1989).

55. Hunt, B. *et al.* Pteropods in southern ocean ecosystems. *Prog. Oceanogr.* **78**, 193–221 (2008).

56. Armstrong, J. L. *et al.* Distribution, size, and interannual, seasonal and diel food habits of northern Gulf of Alaska juvenile pink salmon, *Oncorhynchus gorbuscha*. *Deep. Sea Res. Part II: Top. Stud. Oceanogr.* **52**, 247–265 (2005).

57. Aydin, K. Y., McFarlane, G. A., King, J. R., Megrey, B. A. & Myers, K. W. Linking oceanic food webs to coastal production and growth rates of Pacific salmon (*Oncorhynchus spp.*), using models on three scales. *Deep. Sea Res. Part II: Top. Stud. Oceanogr.* **52**, 757–780 (2005).

58. Karpenko, V. I., Volkov, A. & Koval, M. V. Diets of pacific salmon in the Sea of Okhotsk, Bering Sea, and northwest Pacific Ocean. *N. Pac. Anadr. Fish Comm. Bull* **4**, 105–116 (2007).

59. McLaughlin, K. *et al.* Core principles of the California Current Acidification Network: Linking chemistry, physics, and ecological effects. *Oceanography* **28**, 160–169 (2015).

60. Hauri, C. *et al.* Spatiotemporal variability and long-term trends of ocean acidification in the California Current System. *Biogeosciences* **10**, 193–216, DOI: 10.5194/bg-10-193-2013 (2013).

61. Shchepetkin, A. F. & McWilliams, J. C. The regional oceanic modeling system (ROMS): a split-explicit, free-surface, topography-following-coordinate oceanic model. *Ocean. Model.* **9**, 347–404 (2005).

62. Moore, J. K., Doney, S. C. & Lindsay, K. Upper ocean ecosystem dynamics and iron cycling in a global three-dimensional model. *Glob. Biogeochem. Cycles* **18** (2004).

63. Deutsch, C. *et al.* Biogeochemical variability in the California Current System. *Prog. Oceanogr.* **196**, 102565 (2021).

64. Renault, L. *et al.* Evaluation of high-resolution atmospheric and oceanic simulations of the California Current System. *Prog. Oceanogr.* **195**, 102564 (2021).

65. Armstrong, R. A., Lee, C., Hedges, J. I., Honjo, S. & Wakeham, S. G. A new, mechanistic model for organic carbon fluxes in the ocean based on the quantitative association of POC with ballast minerals. *Deep. Sea Res. Part II: Top. Stud. Oceanogr.* **49**, 219–236 (2001).

66. Wanninkhof, R. Relationship between wind speed and gas exchange over the ocean. *J. Geophys. Res. Ocean.* **97**, 7373–7382 (1992).

67. Kessouri, F. *et al.* Configuration and validation of an oceanic physical and biogeochemical model to investigate coastal eutrophication in the Southern California Bight. *J. Adv. Model. Earth Syst.* **13**, e2020MS002296 (2021).

68. Lewis, E., Wallace, D. & Allison, L. Program developed for CO_2 system calculations. Tech. Rep., Brookhaven National Lab., Dept. of Applied Science, Upton, NY (1998).

69. Sharp, J. D. *et al.* CO2SYSv3 for MATLAB, DOI: 10.5281/ZENODO.3950563 (2020).

Acknowledgements

This research was supported by NOAA grants NA15NOS4780186, NA18NOS4780174, and NA18NOS4780167 (Coastal Hypoxia Research Program), the California Ocean Protection Council grant C0100400NSF, C0831014, and C0303000 (administered by California SeaGrant as R/OPCOAH-1), and the NSF grants OCE-1419323 and OCE-1419450. This work used the Expanse system at the San Diego Supercomputer Center through allocation TG-OCE170017 from the Advanced Cyber Infrastructure Coordination Ecosystem: Serves and Support (ACCESS) program, which is supported by National Science Foundation grants 2138259, 2138286, 2138307, 2137603, and 2138296. Additional computational resources were provided by the Hoffman2 computer cluster at the University of California Los Angeles, Institute for Digital Research and Education (IDRE). Data and code needed to run the ROMS-BEC simulations are available following the link: https://github.com/UCLA-ROMS/Code.

Author contributions statement

CAF conceived and designed the analysis, performed the analysis, and wrote the paper, FK performed the simulations, conceived and designed the analysis, wrote the paper, MH performed the simulations and conceived and designed the analysis, MS conceived and designed the analysis and wrote the paper, DB conceived and designed the analysis and contributed analysis tools, JCW conceived and designed the analysis and contributed analysis tools, CD conceived and designed the analysis and contributed analysis

tools, EH conceived and designed the analysis and contributed analysis tools. All authors reviewed the manuscript.

Figures

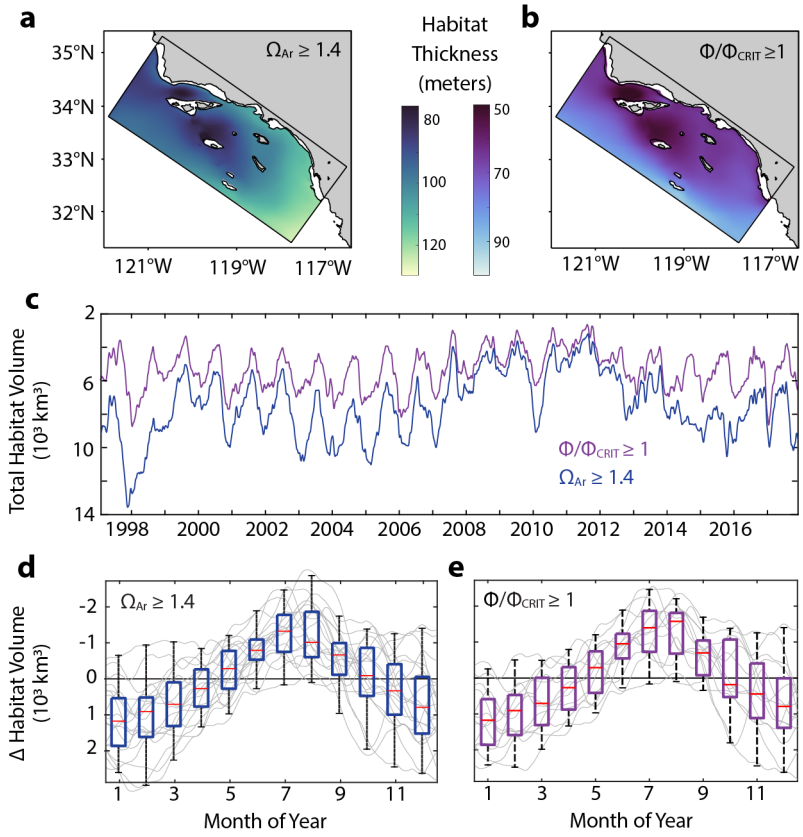

Figure 1. (a-b) Spatial distribution of mean habitat thickness (m) for each biological metric. Coastline and 200-m bathymetric contours (black) shown. Locations within the domain where habitat thickness interacts with seafloor not included. (c) Time-series of total habitat volume (10^3 km^3) summed across the model domain for $\Omega_{Ar} \geq 1.4$ (blue) and $\Phi/\Phi_{CRIT} \geq 1$ (purple). Model output is daily with a two-week running mean applied. (d-e) Seasonal trend in habitat volume for each biological metric. Each annual time-series is detrended with the annual mean (light grey). Box plots (median in red, 25th and 75th percentiles indicated by the bounded box, minimum and maximum as whiskers) for the average monthly values from the annually detrended time series shown (n = 18 years). Y-axes are oriented so that a decrease in habitat volume is upwards and an increase in habitat volume is downwards.

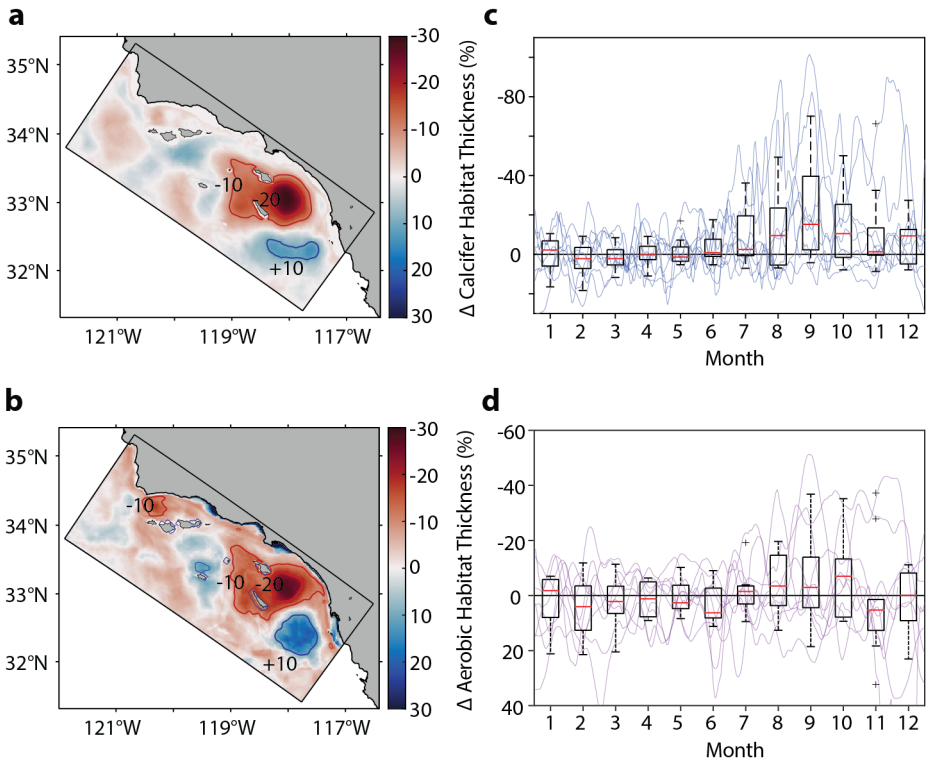

Figure 2. (a-b) Spatial distribution of the percent change in habitat thickness for $\Omega_{Ar} \geq 1.4$ and $\Phi/Phi_{CRIT} \geq 1.0$ between ANTH and CTRL (from average monthly output during time periods of maximum habitat loss, n = 7 events). Thin contours show regions undergoing -10 and +10% change in habitat thickness (red and blue, respectively). Thick red contour shows region experiencing more than -20% change in habitat thickness. (c-d) Seasonal trend of habitat compression within the region undergoing 20% loss in habitat thickness per metric (as contoured in A and B). Individual years (thin lines; n = 9) and box plots of mean monthly percent change in habitat thickness. Y-axes are oriented so that a compression in habitat thickness is upwards and an expansion in habitat thickness is downwards relative to zero.

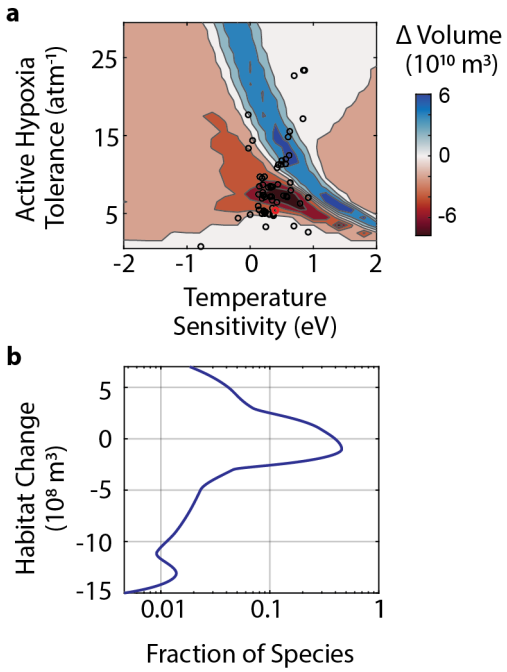

Figure 3. (a) Change in aerobic habitat from land-based nutrient inputs for varied marine ecophysiotypes. The range of Active Hypoxia Tolerance, A_o/Φ_{CRIT}, and temperature sensitivity, E_o, evaluated are based on a global species trait compilation; empirically derived species traits are marked with black circles, northern anchovy is marked with a red circle. Change in aerobic habitat volume assessed for the upper 200 m in the region undergoing 20% habitat compression (see Fig. 2 for region of focus) from months exhibiting maximum compression in the fall (n = 7) due to land-based nutrient inputs. (b) Fitted distribution of the fraction of species (log scale) undergoing trait-weighted volume changes in aerobic habitat. The change in habitat volume weighted by the probability distribution of the empirical traits[3].

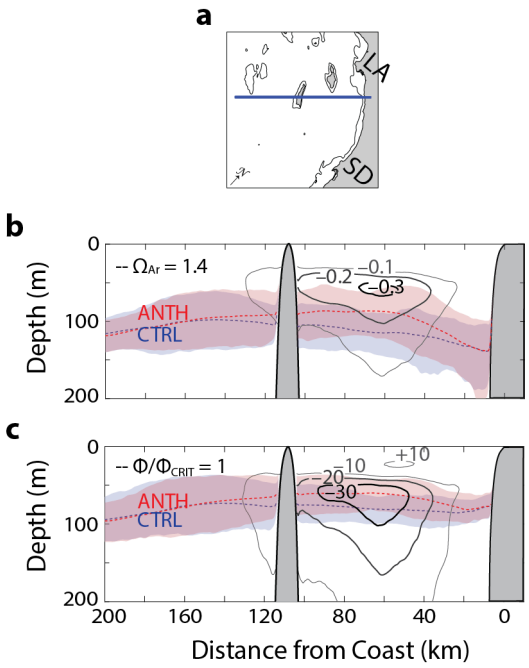

Figure 4. (a) Map of cross-section extending from the coast to 200 km offshore and intersected by San Nicolas Island. Coastline, Los Angeles (LA), San Diego (SD), and 200-m bathymetric contour shown. (b) Cross-section of mean absolute difference (contours) in Ω_{Ar} between the two simulations (ANTH-CTRL) from months exhibiting maximum compression in the fall (n = 7). Contour data overlayed with the mean depth of Ω_{Ar} = 1.4 in the CTRL (blue dashed line) and ANTH (red dashed line) scenario along with 10th and 90th percentiles (shaded blue and red regions, respectively). (c) Same as in (b) but contours are the absolute difference in O_2 (mmol m^{-3}) between ANTH and CTRL overlayed with the mean lower depth limit of Φ/Φ_{CRIT} = 1.

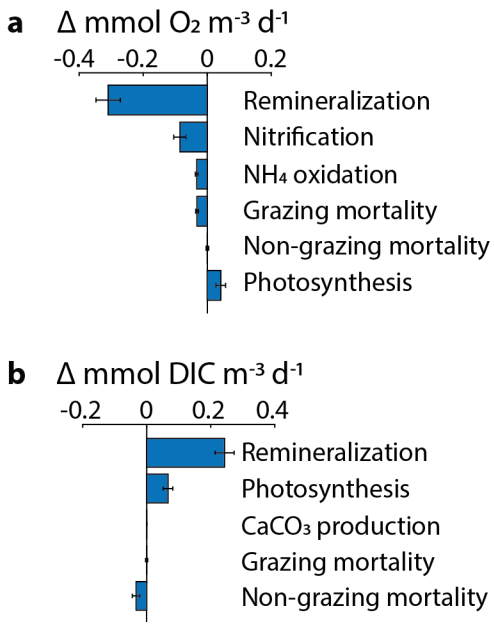

Figure 5. Absolute difference in the biogeochemical rate processes that contribute to the (a) O_2 and (b) dissolved inroganic C (DIC) cycles between the ANTH and CTRL scenarios. Data are monthly averages from within the region of 20% habitat compression (Fig. 2a) averaged from 70 to 140-m water depth (n = 104 months; mean $\pm$ 1 SE).

1 Supplemental Figures

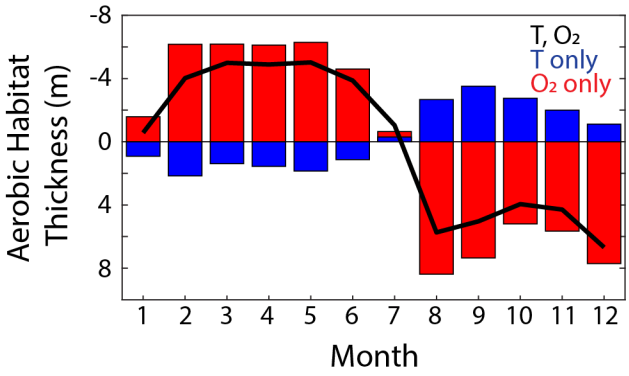

Figure S1. Mean monthly change in Habitat Thickness for $\Phi/\Phi_{CRIT} = 1$ parameterized for northern anchovy (*Engraulis mordax*; $A_O/\Phi_{CRIT} = 5.4$ atm^{-1}, $E_O = 0.4$ eV) calculated from model output 1997-2017 where both temperature and O_2 vary (thick black line), as well as change in habitat thickness due temperature (blue bars) or O_2 (red bars) alone. Y-axis is oriented so that a decrease in habitat thickness is upwards.

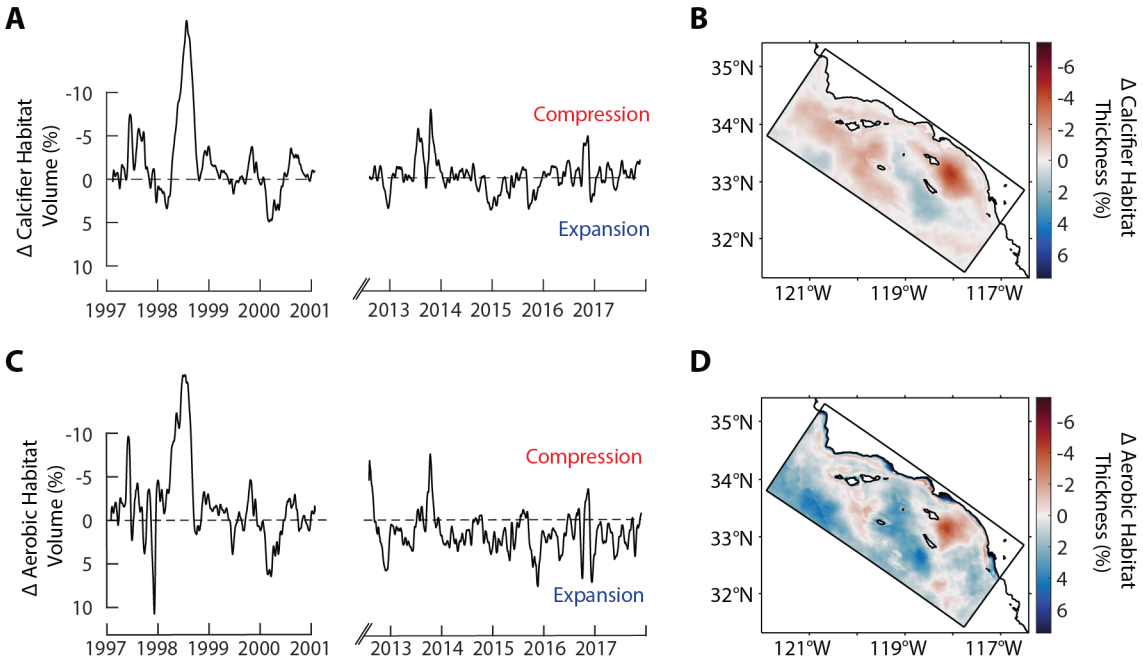

Figure S2. (A,C) Time-series of the percent change between the ANTH and CTRL simulations in total habitat volume averaged across the model domain for $\Omega_{Ar} \geq 1.4$ and $\Phi/\Phi_{CRIT} \geq 1$. Model output is daily with a two-week running mean. (B,D) Spatial distribution of the percent change in habitat volume for $\Omega_{Ar} \geq 1.4$ and $\Phi/\Phi_{CRIT} \geq 1$ averaged across the entire time period of simulations (1998 removed as an outlier year). Coastline and model domain (black outer box) shown. Negative versus positive values indicate time periods or regions undergoing habitat compression versus expansion, respectively, in the ANTH scenario relative to the CTRL scenario. Y-axes are oriented so that a decrease in habitat volume or thickness is upwards.

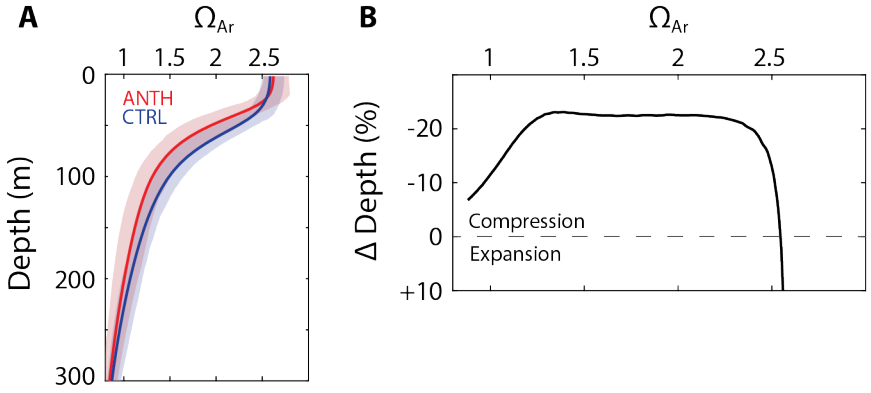

Figure S3. Sensitivity analysis for a range of values of Ω_{Ar} considered suboptimal for calcifiers. (A) Mean aragonite saturation state (Ω_{Ar}) as a function of depth for ANTH (red) and CTRL (blue). Shaded region represents 10th and 90th percentile of conditions. Profile data from Fig. 4 focused on region of maximum impact, averaged 60 – 80 km from shore. (B) Percent change in depth at which a given value of Ω_{Ar} occurs between ANTH and CTRL. Negative values represent a shoaling (compression) of Ω_{Ar} conditions in the ANTH simulation relative to CTRL.

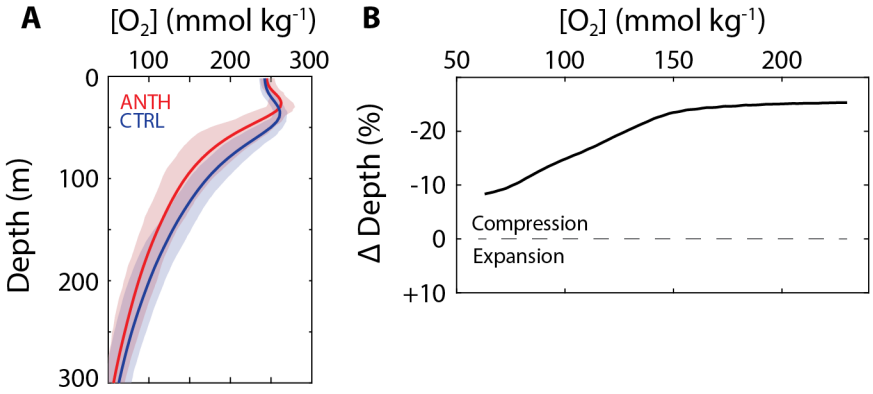

Figure S4. Sensitivity analysis of species parameterization of aerobic habitat. (A) Mean $[O_2]$ as a function of depth for ANTH (red) and CTRL (blue). Shaded region represents 10th and 90th percentile of conditions. Profile data from Fig. 4 focused on region of maximum impact, averaged from 60 – 80 km from the coast. (B) Percent change in depth at which a given value of O_2 occurs between ANTH and CTRL. Negative values represent a shoaling (compression) of $[O_2]$ in the ANTH simulation relative to CTRL. Surface conditions (with increased $[O_2]$ under the ANTH scenario) not included.

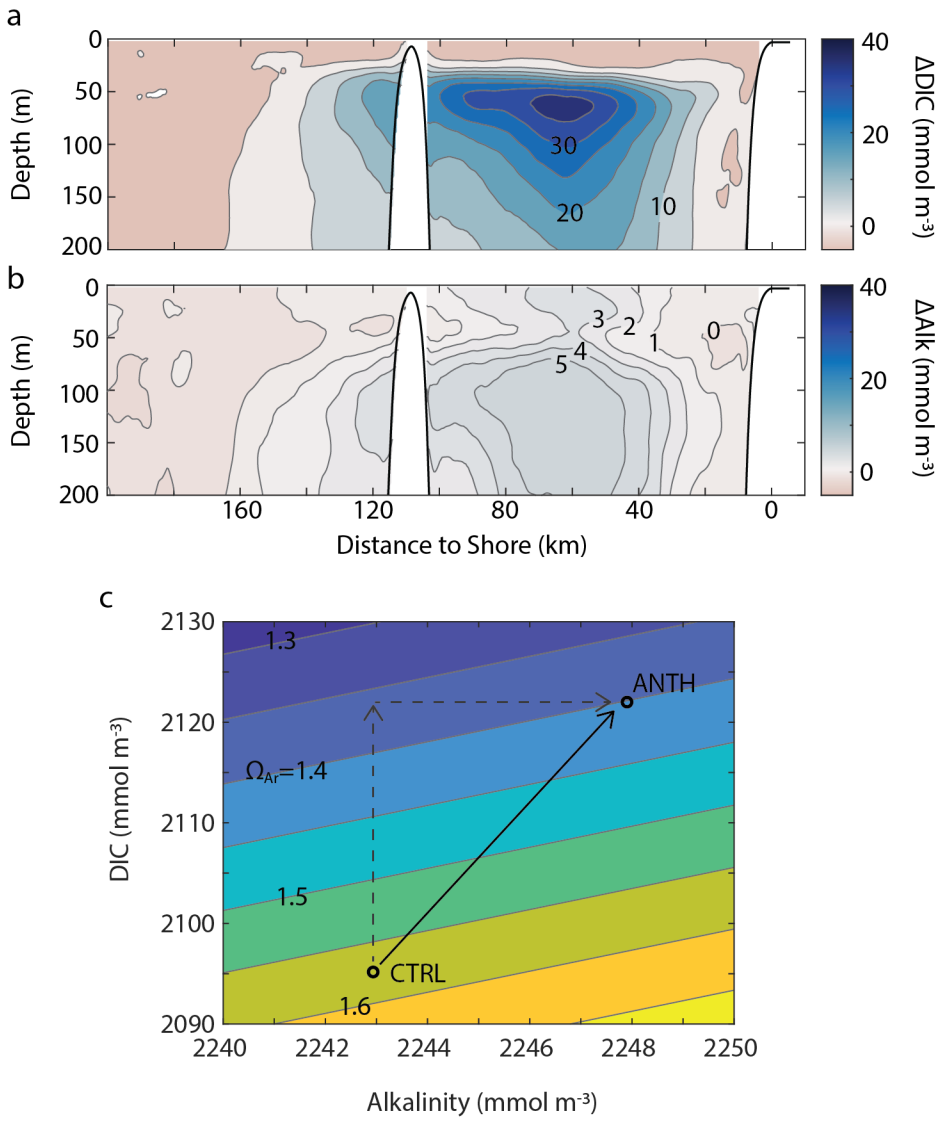

Figure S5. (A-B) Cross-section of mean absolute difference (contours) in dissolved inorganic carbon (DIC) and alkalinity (Alk) between the two scenarios (ANTH-CTRL) from months exhibiting maximum compression in the fall (n = 7). Cross-section plotted as shown in Fig. 4A. (C) Mean alkalinity and DIC in the core of habitat compression (60 – 80 km from the coast and between 30 and 150 m water depth) in the CTRL and ANTH simulation (open circles) along with contours for calculated Ω_{Ar}.T